Measurements of Coherent Cherenkov Radiation in Rock Salt: Implications for GZK Neutrino Underground Detector

R. Milincic, P. W. Gorham, and E. Guillian
Dept. of Physics & Astronomy, Univ. of Hawaii at Manoa, 2505 Correa Rd. Honolulu, HI, 96822
D. Saltzberg and D. Williams
Dept. of Physics & Astronomy, Univ. of Calif. at Los Angeles, Los Angeles, CA
R. C. Field and D. Walz
Stanford Linear Accelerator Center, Stanford University, Menlo Park California

We report on further SLAC measurements of the Askaryan effect: coherent radio emission from charge asymmetry in electromagnetic cascades. We used synthetic rock salt as the dielectric medium, with cascades produced by GeV bremsstrahlung photons at the Final Focus Test Beam. We extend our prior discovery measurements to a wider range of parameter space and explore the effect in a dielectric medium of great potential interest to large scale ultra-high energy neutrino detectors: rock salt. We observed strong coherent pulsed radio emission over a frequency band from 0.2-15 GHz. A grid of embedded dual-polarization antennas was used to confirm the linear polarization and track the change of direction of the electric-field vector around the shower. Coherence was observed over 4 orders of magnitude of shower energy. The frequency dependence of the radiation was tested over two orders of magnitude of UHF and microwave frequencies. Based on these results we have performed a simulation of a realistic GZK neutrino telescope array within a salt-dome, and we find it capable of detecting 10 or more contained events per year from even the most conservative GZK neutrino models.

1. Introduction

It is understood that the universe becomes opaque to photons above 100 TeV due to pair production on the cosmic infrared and microwave background [1]. Stable charged baryons or leptons do not become magnetically rigid enough to propagate over intergalactic distances until their energies are so high that they also suffer significant losses through interactions with the cosmic microwave background , through the process first noted by Greisen, and Zatsepin & Kuzmin (GZK) in the early 1960's [2, 3].

Extragalactic astronomy in the 10^{15-21}eV energy range at $\geq$ 0.1 Gpc scales must therefore utilize other messengers, and neutrinos are the most likely contender. Moreover, the existence of sources that can produce single particles with energies approaching 1 Zeta-electron-volt (10^{21}eV= 1 ZeV = 60 Joules) provides a compelling driver toward development of ultra-high energy neutrino detectors. This goal compels us to consider detectors with target masses approaching 10^{42} nucleons, a Teraton of mass at EeV energies [4]. A promising approach toward this task is to utilize the Askaryan effect [5], a process which leads to strong, coherent radio pulses from such cascades. Antarctic ice has been the focus of studies for this goal for several years now via the Radio Ice Cerenkov Experiment (RICE) [6], and the Antarctic Impulsive Transient Antenna (ANITA) [7].

Rock salt, first suggested as a possible target medium by Askaryan [5], is the focus of recent efforts, and it shows promise for detector development. We report here on experiments to further understand aspects of the Askaryan process in rock salt as the medium for the cascades and radio pulse production. Our results now extend measurements of the effect over the entire range of cascade energies and radio frequency range of interest for GZK neutrino detection. We made the first measurements of the vector change of polarization at different locations around the shower axis. These results open the road to Teraton neutrino detectors.

2. Experimental setup

The experiment (SLAC T460) was performed at the Final Focus Test Beam (FFTB) facility at SLAC in June 2002. As in our first SLAC measurement [10], we used gamma-rays from Aluminum radiators of different thicknesses to provide secondary bremsstrahlung gamma-rays for shower production in our rock salt target. The geometry of the target is shown in Fig. 1. It was built of 1.8 kg salt bricks, with a total mass of about 4 metric tons. The bricks are slightly trapezoidal in all of their cross sections, but have average dimensions of $15 \times 10 \times 6$ cm, and specified to be at least 99.5% pure sodium chloride. Their density was measured to be 2.08 g cm^{-3}. The implied upper limits on the attenuation length $L_\alpha = \alpha^{-1}$ are hundreds of meters [11] in the UHF and cm wave regime, so we assume negligible bulk absorption of the radio emission in the results reported here. An array of 7 by 3 (21 total) printed-circuit board (PCB) broadband dual-linear-polarization bowtie antennas was embedded in the upper portion of the target, on a rectangular grid with spacings of 22 cm along the shower axis and 21 cm transverse to it, with one set of antennas arranged with one of their polarization axes aligned directly above the beamline. These are shown schematically

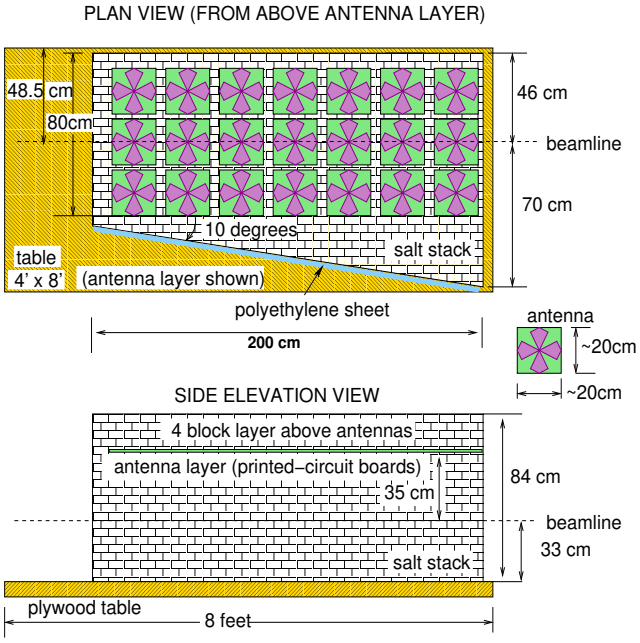

Figure 1: Geometry of the salt-block shower target used in the experiment.

in Fig. 1. The antennas had a frequency response of approximately 0.2-2 GHz, and about -12 dB of cross-polarization rejection. In addition, we used two external antennas: a C/X-band horn (frequency range from 5 to 9 GHz), and a 1-18 GHz log-periodic dipole array (LPDA) antenna at location on the side of the target.

A 2.5 cm thick polyethylene sheet was arranged with a 10° angle with respect to the beamline to facilitate transmission of the Čerenkov radiation, which would have otherwise been totally internally reflected from a parallel face.

Antenna signals were digitized with oscilloscopes using a microwave transition-radiation-based trigger from an upstream location. The shower energy was varied by changing both the electron beam intensity and the thickness of the bremsstrahlung radiators. These radiators varied from 0.06% to 1.5% of a radiation length. The electrons were then steered away from the salt target and dumped into the FFTB beam dump approximately 20 m downstream. SLAC beam current monitors allowed us to reduce beam intensity to about 10^9 electrons per bunch using conventional methods. However, by employing our coherent microwave transition radiation trigger, we were able to further monitor the beam intensity to levels an additional 2 orders of magnitude below this, and with the combination of radiators available to us, the dynamic range of the showers obtained was thus about 4 orders of magnitude in shower energy.

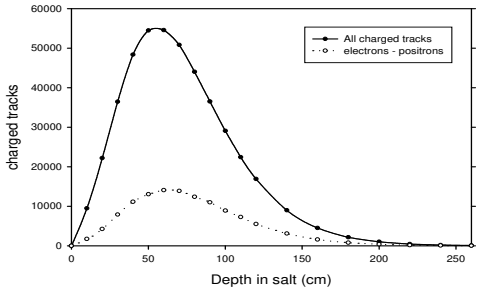

Figure 2: Longitudinal distribution of the bremsstrahlung shower, for both total charge and charge excess as simulated by EGS4 for rock salt.

3. Results

To provide a baseline for evaluation of the results, we simulated the electromagnetic showers using the Electron Gamma Shower 4 (EGS4) code [12]. Figure 2 shows the longitudinal shower development for a salt target, including the charge excess. The $\sim 25\%$ negative charge excess demonstrates that the Askaryan effect is generic to electromagnetic showers. The simulation is for 1000 28.5 GeV electrons initially, led through a 10% bremsstrahlung radiator to fully account for the secondary photon spectrum.

3.1. Coherence & Absolute Field Strength.

The measurements of coherence were made using averaged results from several of the bowtie antennas around the region of shower maximum. Typical runs at a given total charge per bunch were averages of 1000 beam shots, and the beam current was separately monitored for stability. Typically we also recorded 100-1000 shot-to-shot pulse profiles to monitor the variance. Fig. 3 shows the results of the relative radio-frequency power as a function of shower energy, now covering nearly 4 orders of magnitude in energy and 8 orders of magnitude in RF power. No departures from the expected quadratic dependence of pulse power with shower energy are seen. This result demonstrates the remarkable dynamic range for detection of coherent RF Čerenkov radiation.

Determination of the absolute measured field strength of the showers requires that the antenna effective area, spectral response, coupling efficiency, and angular response all be included in converting the measured voltages to field strengths in the detection medium. For the antenna as a receiving component, with: the distance source to antenna ($R = 38$ cm), the largest antenna dimension ($L = 20$ cm), and $\theta = 25°$ at the Čerenkov angle the antenna far field conditions are satisfied for frequencies below 2 GHz, the highest usable frequency for the bowtie antennas. Antennas

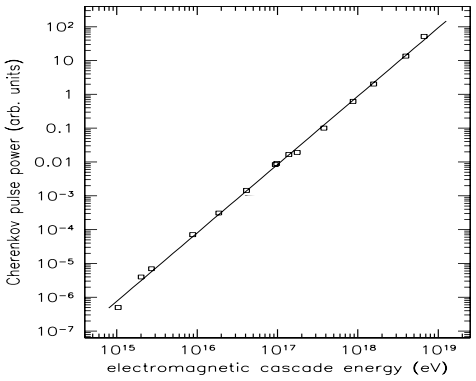

Figure 3: Observed coherence of the 0.3-1.5GHz radiation as a function of total beam energy per pulse. The curve shows a quadratic relation for power as a function of shower energy.

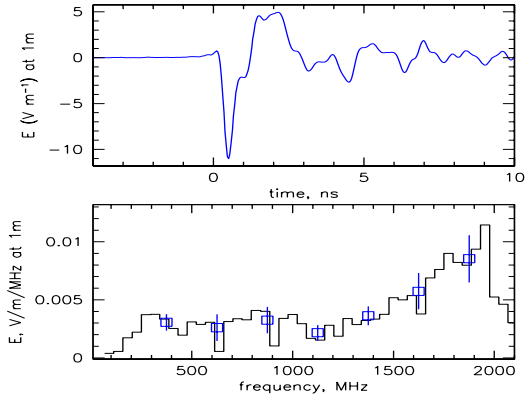

Figure 4: Top: Summed-in-phase pulse profile from all bowtie antennas. Bottom: Absolute power spectrum of the bowtie data, corrected for antenna angular response.

receive radiation only from approximately that portion of the shower that is projected onto the antenna effective area at the Čerenkov angle. This behavior was observed in ref. [10], and provides the possibility of tracing out the longitudinal charge evolution of the shower by measuring the change in radiation amplitude along the shower axis, as was done in ref. [10] (see also Fig. 7 below).

Figure 4(top) shows a plot of the summed field strengths from all of the bowtie antennas, corrected for cable attenuation but not for other frequency dependent effects. In the bottom portion of the figure, a Fourier amplitude spectrum of the field strength is shown, including corrections for the gain of the bowtie antennas. The solid histogram shows the power spectrum of the pulse, and the points are averages over 250 MHz sections of the spectrum, with the error bars based on the spectral variance within each section. It is evident that there are some near-nulls in the bowtie response, but the overall trend is for a rise

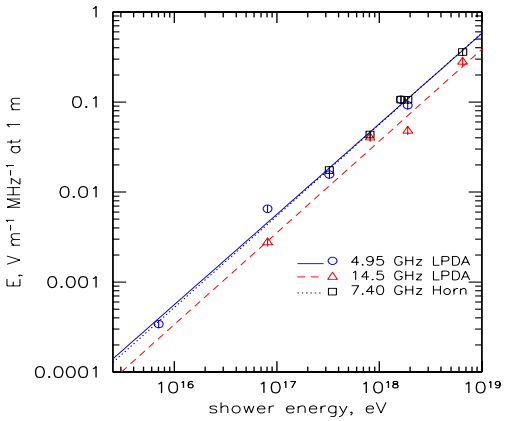

Figure 5: Measured coherence of electric field strength at 4.95, 14.5 with LPDA and 7.4 GHz with horn antennas respectively, with least-squares fit curve.

at the higher frequencies, consistent with Čerenkov radiation.

We also measured the coherence at higher frequencies (2.2-15.0 GHz) in several bandpasses, using the LPDA and the C/X-band horn antennas, both of which had known effective areas. Fig. 5 shows the measured electric field strength vs. total shower energy at different frequencies. Measurements were done with the LPDA on 4.95 and 14.5 GHz, respectively and with the horn antenna at 7.4 GHz. Points represent measured values and lines are least-square fit curves $|\mathbf{E}| = AE_{sh}{}^{\alpha}$, where $\mathbf{E}$ is the electric field and E_{sh} the shower energy. The fit for the exponent α gives: $\alpha_{4.95} = 1.00 \pm 0.04$ at 4.95 GHz, $\alpha_{14.5} = 1.02 \pm 0.11$ at 14.5 GHz, $\alpha_{7.4} = 0.99 \pm 0.05$ at 7.4 GHz. On all three frequencies, the field strength is in agreement with full coherence of the radiation.

Fig. 6 shows the absolute field strength measured in several frequency bands from 0.3-15.0 GHz. The plotted curve is based on the parametrization given in [13], scaling from ice to synthetic rock salt. The horizontal bars are not standard errors but show antenna or filter bandwidth, and vertical bars indicate combined statistical and systematic uncertainties.

3.2. Polarization and charge excess tracking

The crossed bowtie antennas provided simultaneous measurements of the induced voltage in orthogonal linear polarizations. Since each of the bowtie antennas are identical in both the co- and cross-polarized directions, and since the induced voltage has a simple sinusoidal dependence on the projected plane of polarization angle Ψ, we can write

$$V_0 = Eh(\cos\Psi + \alpha \sin\Psi) \qquad (1)$$

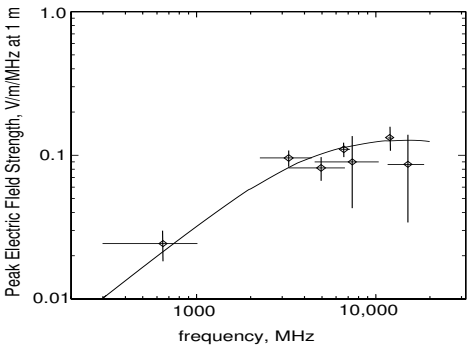

Figure 6: Spectral dependence of the measured electric field strength for shower energy $1.9 \times 10^{18} eV$. The solid curve is a simulation scaled for synthetic rock salt. Vertical bars are estimated errors, largely due to systematics in the absolute RF calibration; horizontal bars indicate the bandwidth used.

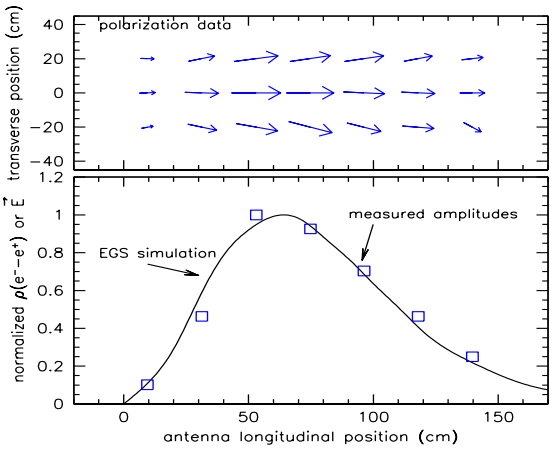

Figure 7: Top: Measured polarization vector field at the bowtie antenna locations. Bottom: The observed amplitude of the received RF pulses along the center line of the antenna array. Curve is an EGS simulation of showers; both curves are normalized.

$$V_{90} \;=\; Eh(\sin\Psi + \alpha\cos\Psi) \qquad (2)$$

where $h = \frac{1}{2}(|h_0| + |h_{90}|)$ has the same magnitude for both the co- and cross-polarized antennas.

The co-polarized direction was aligned with the beam axis. When Ψ is approximately aligned with the beam axis, then for an antenna along that axis, we find that $\alpha = (V_{90}/V_0)|_{on-axis}$. Ψ is then determined by

$$\Psi = -\tan^{-1}\left(\frac{\alpha - V_{90}/V_0}{\alpha V_{90}/V_0 - 1}\right) . \qquad (3)$$

Fig. 7 shows results of the polarization and relative amplitude measurements for all bowtie antennas. The top pane plots these as vectors with scaled lengths and directions corresponding to the square root of the amplitude and the projected plane of the polarization Ψ. In the lower pane of the figure, we also show the relative amplitude of the antennas along the center axis as a function of the longitudinal distance along the shower (corrected for the Čerenkov angle projection). We also plot the EGS4 simulation of the shape of the charge excess along the shower. There is excellent agreement between the measured shape of the amplitude response and the normalized charge excess predictions from EGS4.

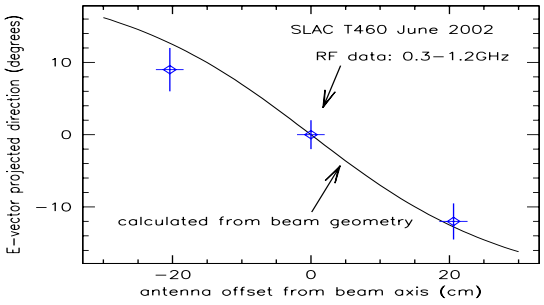

Figure 8: Plane of polarization vs. transverse distance of the antennas, which were all about 35 cm above the axis of the beam.

In Figure 8 we show similar data for the three antennas at shower maximum at a depth of 50 cm, now plotting the plane of polarization as a function of the transverse position of the antenna with respect to the centerline of the beam. The solid curve shows the expected change in the angle of polarization for the three antennas, and the agreement is good.

4. Discussion

Our radio Čerenkov measurements demonstrate conclusively that coherent Čerenkov radio pulses from showers in the rock salt can accurately reconstruct the profile of the shower development as well as the total shower energy. They show that the process is inherently quadratic in the rise of power vs. shower energy, and this relationship is reliable over many decades of these parameters. Combining these results with *in situ* measurements of propagation characteristics at radio frequencies in salt domes [9] which indicate $\geq$ 250 m attenuation length, we conclude that nothing in principle prevents the development of embedded antenna arrays within large salt structures such as salt domes for the characterization of ultra-high energy neutrino fluxes.

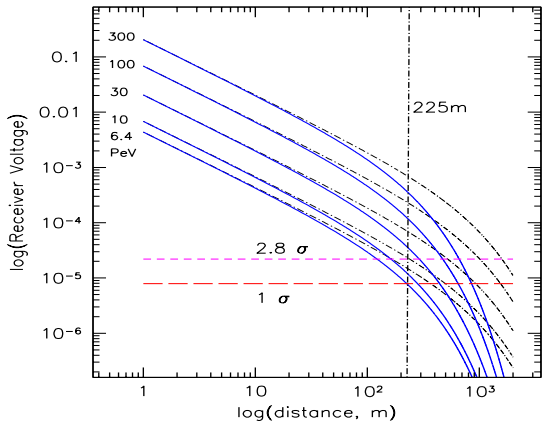

Figure 9: Detection threshold estimates for a Saltdome Shower Array (SalSA). Solid & dashdot curves show received voltages as a function of distance for a 250 m (solid) and 900 m (dashdot) attenuation lengths, for the energies marked at left. The $1, 2.8\sigma$ noise levels shown are for a 450 K system temperature. The 225 m line is the antenna node spacing.

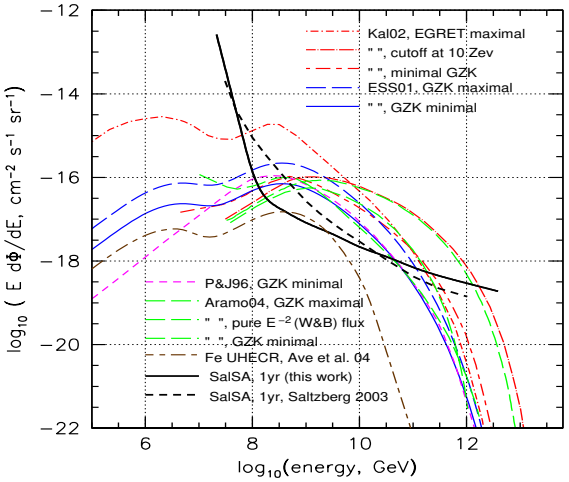

Figure 10: Estimated sensitivity for a SalSA for one year of exposure. A set of GZK models is shown, as well as an earlier estimate of SalSA sensitivity [19].

4.1. Application to detector modeling.

We have created a MC simulation of a large-scale antenna array embedded in a salt dome. We denote the array here as a Salt dome Shower Array (SalSA). The array is cubic with 1728 antenna nodes ($12 \times 12 \times 12$), with a grid spacing of 225 m, based on conservative estimates [9] of the attenuation length in rock salt.

Each node consists of 12 closely spaced antennas (0.75 m vertical offset), 6 of which are dipoles with vertical polarization, and 6 of which are slotted-cylinder antennas which are sensitive to horizontal polarization. The antennas are both assumed to have $\cos^2\theta$ response functions. The antennas are optimized for frequencies centered at about 200 MHz, with bandwidth of about 100%. A system temperature of 450K is assumed, based on about 310K for the salt and a receiver noise temperature of 140K, consistent with low-noise amplifiers.

For triggering, an event must produce a voltage magnitude above 2.8σ on 5 of 12 of the local antennas within a node. This threshold and coincidence level is chosen to reduce the accidental rates. The five 2.8σ signals yield a joint probability corresponding to 5.7σ, and even assuming one of the five is excluded for any reason, the remaining four signals have a joint 5σ probability.

4.1.1. Simulation results.

Figure 9 shows the dependence of the received voltage, based on the parametrization of reference [13], scaled for salt, as a function of distance and shower energy. The curves are labeled by shower energy in PeV, and both the 1σ and 2.8σ levels for rms voltage above the baseline noise level are shown. The solid and dash-dot curves are for $L_\alpha = 250,\ 900$ m respectively.

The 225 m spacing will give a shower energy threshold in the neighborhood of 30 PeV for assumption of $L_\alpha = 250$ m, and in practice we find that other loss factors and the neutrino interaction Bjorken y-factor contribute to push the optimal sensitivity to neutrino energies of order 100 PeV. Figure 9 indicates that, although it may be possible to operate a SalSA at a low enough energy threshold to detect events at the 6.4 PeV Glashow Resonance for W-vector boson production via $\nu_e + e^- \to W^-$, the node spacing required is below 100 m, implying an order of magnitude more array elements. In addition, the GZK neutrino spectrum peaks above ~ 100 PeV. The volume enclosed by the simulated array is approximately 15.6 km^3 of salt, or about 34 km^3 water equivalent mass. An additional 11.4(63) km^3 (24.9(137) km^3 w.e.) is contained in one attenuation length (for $L_\alpha = 250(900)$ m) of the outer wall. The effective fiducial volume thus approaches 60(170) km^3 w.e.. The solid angle acceptance is upper 2π hemisphere, and extends about $10 - 15^\circ$ below the horizon, depending on neutrino energy. This implies of order 400(1190) km^3 sr w.e. acceptance, with a threshold of order 10^{17} eV or less.

The simulation is performed using an isotropic neutrino flux, and integrating through a shell-density model for the earth to determine the angular distribution of neutrinos in the detector. We use a 1:1:1 $e : \mu : \tau$ mix of neutrino flavors. For the radio emission, the Zas-Alvarez-Muñiz parametrization [13] is used.

4.1.2. Estimates of GZK neutrino event rates.

We assumed a monoenergetic neutrino flux at discrete energies over the PeV to ZeV. The inverse of the exposure gives the model-independent flux sensitivity using the procedure outlined in ref. [15].The result of this estimate for the flux sensitivity for 1 year of exposure is shown in Fig. 10, plotted along with various estimates of GZK neutrino fluxes [16, 17, 18]. A model which just equaled the sensitivity curve for one decade of energy would give about 3 events. Also plotted is an earlier SalSA sensitivity estimate [19] with a simpler detector model.

For the three minimal GZK models shown the expected rates are about 11-14 events per year. For the highest GZK neutrino models in which all parameters are maximized subject only to firm observational constraints such as the EGRET gamma-ray limits, the possible event rates are up to 120 per year.

For a system with a design lifetime of 10 years or more, even minimal GZK neutrino fluxes will produce a rich data sample. Increases in neutrino cross sections above the standard model, like from the effects of microscopic black hole production in theories with large extra dimensions [21], would yield much larger event rates than described here.

5. Conclusions

We conclude the following from our measurements and simulations:

1. The Askaryan effect behaves as theoretically expected in measurements made in synthetic rock salt. Correlation of the strength of the radiation to the estimated charge excess is excellent.

2. The polarization properties of the observed radio emission are consistent with coherent Čerenkov radiation, and can be used to derive geometric properties of the shower track to good precision.

3. The observed radiation is completely coherent over many decades of shower energy, and a wide range of radio and microwave frequencies.

4. An antenna array of order 2.5 km on a side in an underground salt dome is well able to conclusively detect and characterize all current standard model GZK neutrino fluxes on even a 1 year time scale; over 10 years of operation, good statistics can be obtained on the GZK neutrino spectrum above 10^{17} eV.

Acknowledgments

We thank the staff of the Experimental Facilities Division at SLAC for their support of our efforts, M. Rosen at the Univ. of Hawaii; D. Besson, J. Learned, A. Odian, and W. Nelson for advice and useful discussion. This work was performed in part at the SLAC, under contract with the US Dept. of Energy, and at UCLA under DOE contract DE-FG03-91ER40662, and under DOE contract DE-FG03-94ER40833 at the University of Hawaii.

References

[1] F. Halzen *et al*, Phys. Rev. D 4, 342 (1990); J. Wdowczyk & A. W. Wolfendale, Ap. J. 349, 35 (1990).
[2] K. Greisen , 1966, Phys. Rev. Lett., **16**, 748.
[3] G. T. Zatsepin & V. A. Kuzmin, Pis'ma Zh. Eksp. Teor. Fiz. 4 (1966) 114 [JETP. Lett. 4 (1966) 78]. Sov. J. Nucl. Phys. 11, 111 (1970);
[4] D. Seckel & G. Frichter, Proc. 1st Int. Workshop Rad. Detect. High Energy Part. (RADHEP 2000), ed. Saltzberg & Gorham , (AIP press) (2001).
[5] G. A. Askaryan,1962, JETP 14, 441
[6] I. Kravchenko et al., Astropart.Phys. 20 (2003) 195-213.
[7] A. Silvestri,*et al*, (2004) astro-ph/0411007
[8] M. Chiba *et al*, (2004) Phys. Atom. Nuclei 67(11), 2050.
[9] P. Gorham *et al*, NIM A490, 476, (2002).
[10] D. Saltzberg, P. Gorham, D. Walz,*et al*, 2001, Phys. Rev. Lett., **86**, 2802.
[11] A. von Hippel, editor, *Dielectric Materials and Applications*, (1995 ed.), Artech House.
[12] W. R. Nelson *et al*, SLAC-265, 1985.
[13] J. Alvarez–Muñiz, & E. Zas, 1997, Phys. Lett. B, 411, 218
[14] J. D. Kraus, 1988, *Antennas*, (McGraw-Hill:New York)
[15] L. A. Anchordoqui, *et al*, Phys. Rev. D66 (2002) 103002.
[16] O. E. Kalashev *et al*, Phys. Rev. D **66**, 063004 (2002).
[17] R. J. Protheroe & P. A. Johnson, Astropart. Phys. 4 (1996) 253.
[18] C. Aramo, *et al*, 2004, Astropart. Phys., in press; astro-ph/0407638.
[19] D. Saltzberg, *et al*, (2003), Proc. SPIE conf. 4858, Part. Astroph. Instrum., P. Gorham, ed., (SPIE: Bellingham, WA), 191.
[20] E. Waxman and J. N. Bahcall,
[21] J. L. Feng & A. D. Shapere, Phys. Rev. Lett. 88, 021303 (2002); J. Alvarez-Muniz *et al*, Phys.Rev. D65 (2002) 124015.